Laves Phases

DOI: 10.1002/anie.201001534

Structural Topology and Chemical Bonding in Laves Phases**

Alim Ormeci, Arndt Simon, and Yuri Grin**

The nature of the atomic interactions in intermetallic compounds is continuously under investigation.[1,2] Different techniques are applied for the analysis of the chemical bonding in this class of inorganic compounds; for example, deep insights into the building up of the complex crystal structure of $NaCd_2$ were obtained by extended Hückel and DFT (LDA) calculations.[3] Laves phases comprise an enormous number of intermetallic compounds with general composition MN_2 and multicomponent derivatives. They were thought to be understood in respect of the factors influencing their formation. Early on, a geometric rule for stability as well as an electronic rule for the occurrence of certain structural variations, for example cubic versus hexagonal variants, have been developed. The geometric rule[4–6] based on a common close-packing of hard spheres with different sizes identified an "ideal" radius ratio $r_M/r_N = \sqrt{3/2} = 1.225$ as a necessary condition for the formation of this family of structures. The only then-known alkali metal phase KNa_2[7] supported the validity of this rule: The radius ratio $r_K/r_{Na} = 1.24$ for the chemically very similar metals K and Na closely matches the ideal value.[8] As to the electronic rule, it was claimed that the valence electron concentration (VEC) is the crucial factor defining the variety of the crystal structures of the Laves phases. In a theoretical study, both electronic and size factors were found to be important.[9] Later critical assessment of the literature data[10] revealed in particular that the maximal numbers of Laves phases are formed at the radius ratios of 1.15 and 1.30, and, moreover, at the "ideal" value of 1.225 only few representatives are found. The first attempts to analyze chemical bonding were made within the tight binding and extended Hückel formalisms;[11,12] later, quantum chemical studies based on augmented plane waves method were performed.[13] Experimentally, evaluation of the charge density from the diffraction data was attempted.[14]

In a Pearson diagram, the "ideal" radius ratio is identified as the condition of strain-free M–N and N–N contacts with respect to the atomic radii r_M and r_N of the elements.[15] However, the distribution of actual structures in the Pearson diagram does not take too much notice of such strain-free contacts, particularly when elements of very different chemical character such as potassium and bismuth are combined. The discovery of additional Laves phases of the alkali metals, $CsNa_2$[16] and CsK_2,[17] clearly indicated that the radius ratio $r_M/r_N = 1.43$ and 1.15, respectively, can deviate significantly from the "ideal" value even in the case of very similar metals, which agrees well with the conclusions of reference [9]. The interatomic distances d_{ij} of these three inter-alkali phases strictly follow a linear relationship, which corresponds to a Vegard-type law [Equation (1)]:

$$d_{ij} = F_{ij}(r_M + 2r_N) \quad (1)$$

where factors F_{ij} are defined by geometrical features of the structures based on the closest packing of spheres of different size.[17,18] A theoretical basis for this relationship is given in reference [19]. The atomic radii r_M and r_N are derived from the observed distances in the respective elements and normalized to the coordination number CN = 12. Taking into account the different coordination numbers of the M and N atoms in the Laves phases, a general relation [Equation (2)]

$$(2r_M - d_{MM})/2r_N = 0.6450\, r_M/r_N - 0.7670 \quad (2)$$

has been derived, where d_{MM} is the shortest distance between the M atoms.[18] The equation describes the structure of Laves phases as the closest packing of spheres with different sizes, and holds for the cubic and the hexagonal variants provided the latter have the ideal c/a ratio of $\sqrt{8/3}$. Numerous phases formed from chemically not too different metals closely follow Equation (2) (Figure 1), which also shows some compounds deviating strongly from it.[18,20,21]

Thus, the position of compounds in a Pearson diagram in respect to Equation (2) may serve as a guideline for the analysis of chemical bonding in the only seemingly homoge-

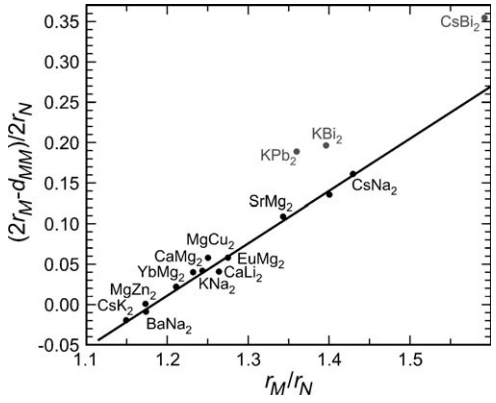

Figure 1. Pearson diagram for selected Laves phases. The solid line corresponds to the Equation (2).

[*] Dr. A. Ormeci, Prof. Yu. Grin
Max-Planck-Institut für Chemische Physik fester Stoffe
Nöthnitzer Strasse 40, 01187 Dresden (Germany)
Fax: (+49) 351-4646-4002
E-mail: grin@cpfs.mpg.de
Prof. Dr. A. Simon
Max Planck Institute for Solid-State Research
Heisenbergstrasse 1, 70569 Stuttgart (Germany)
Fax: (+49) 711-689-1642
E-mail: a.simon@fkf.mpg.de

[**] We are grateful to Roald Hoffmann for valuable discussions, and we thank Victor Bezugly for the calculations on Pb_4^{4-}.

neous family of Laves phases, which comprises in its extremes intermetallic compounds with low difference in electronegativities between the components and rather salt-like species with large difference in electronegativity.

This was the starting point for our consideration of the bonding features in Laves phases. To visualize similarities and differences in the bonding of Laves phases, we analyzed several representatives in terms of electron localizability and electron density. The first attempt of such analysis of a Laves phase $CaAl_2$ was made[22] using the idea of electron localization function.[23] The local maxima of ELF were found between the aluminum atoms and also aluminum and calcium atoms, indicating a bonding different from the elemental aluminum. We use the electron localizability indicator (ELI[24]) for the evaluation of the atomic interactions in Laves phases. The ELI was initially designed to depict the position-dependent fraction of a same-spin electron pair per fixed, sufficiently small charge enclosed in compact regions (microcells) in space and was therefore denoted as ELI-q. Another variant of the ELI, named ELI-D, depicts the position-dependent average number of electrons per fixed fraction of a same-spin electron pair.[24] Deviations from the spherical distribution of ELI for the noninteracting atoms may appear in chemical compounds in the form of local maxima (attractors) between the atoms or in form of the structuring of their inner shells; both features are fingerprints of the atomic interactions.[26] Hereafter we use ELI-D and refer to it as ELI. The results of the calculations for selected representatives of Laves phases are presented in Figure 2 (distributions of ELI in the $(11\bar{2}0)$ plane) and Figure 3 (isosurfaces of ELI).

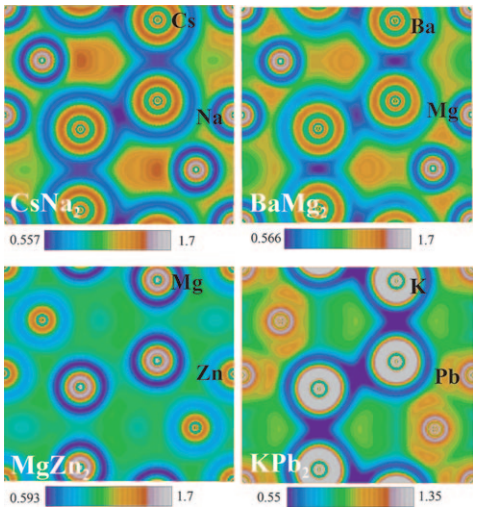

Figure 2. Electron localizability indicator in the Laves phases $CsNa_2$, $BaMg_2$, $MgZn_2$, and KPb_2. ELI distributions in the $(11\bar{2}0)$ planes are shown together with the color scale for ELI values of each compound.

In Laves phases formed solely from alkali metals, for example KNa_2, CsK_2, and $CsNa_2$, ELI is characterized by a spherical distribution in the inner shells of atoms, indicating that the electrons of these shells do not participate in the bonding within the valence region, in accordance with

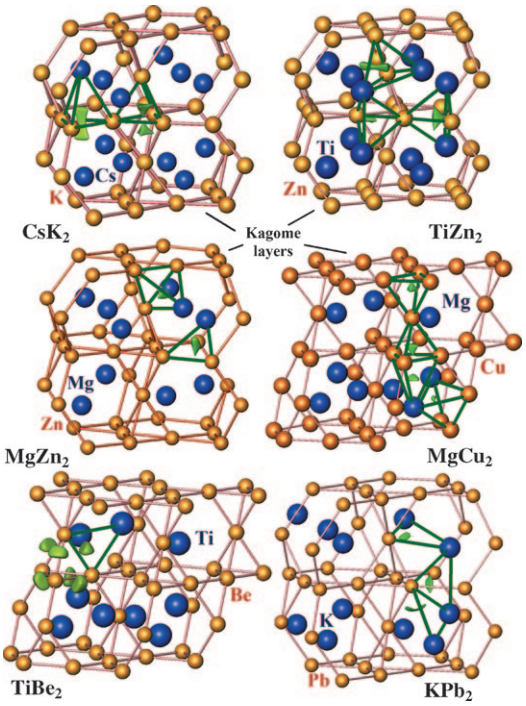

Figure 3. ELI isosurfaces visualize the positions of the ELI attractors and reveal multicenter bonding in selected Laves phases.

expectation (Figure 2 for $CsNa_2$). Two types of ELI maxima are present; topological analysis shows that these have polysynaptic basins.[25] The first type is located inside the tetrahedra N_4, and the second is positioned within the tetrahedra MN_3 visualizing the four-center interactions (Figure 3 for CsK_2).

By increasing VEC we come to $BaMg_2$ (Figure 2). In this case there are three sets of ELI attractors; all are close but shifted off-center from the N–N contacts. All three stand for the multicenter M–N bonding. Two sets visualize four-center M_2N_2 (or in more strict sense six-center M_4N_2) bonds. The third set is located in front of the edges of the bipyramids of the tetrahedral network representing three-center bonds MN_2 (or in a more strict sense the five-center bonds M_3N_2).

Introducing transition metals leads to more complex ELI topologies in the Laves phases. In both prototypes, $MgZn_2$ and $MgCu_2$, ELI reveals a similar picture: The inner shells of copper and zinc are not structured (see Figure 2 for $MgZn_2$). Similar to $BaMg_2$, the ELI attractors are positioned in the tetrahedra N_4, M_2N_2 and MN_3, revealing multicenter interactions (Figure 3 for $MgZn_2$ and $MgCu_2$).

Two representatives of titanium containing Laves phases, $TiZn_2$ and $TiBe_2$, differ strongly in the topology of ELI (Figure 3). The fact that the inner shells of titanium are not markedly structured is unexpected in the first instance and signalizes the participation of only the fourth-shell electrons in the bonding with beryllium or zinc. The maxima of ELI in $TiZn_2$ are located in the mixed tetrahedra, as in the magnesium compounds. Despite the same number of valence electrons, the ELI distribution in $TiBe_2$ is simpler than in $TiZn_2$. The attractors are positioned within the triangles MN_2 (or in a more strict sense in the bipyramids M_3N_2), are but

very close to the *N*–*N* contacts. Dominance of *N*–*N* contacts in the bonding situations of C14 phases has already been emphasized.[12]

In the ELI representation of KPb_2 (Figure 2 and Figure 3), no distinct attractors are found between potassium and the framework. A single set of ELI attractors is observed; all of them are located in the last shell of the *N* atoms (six attractors per *N* atom). Formally the corresponding basins are trisynaptic (three-center M_2N bonds; Figure 3), but their location in the outer shell of lead atoms implies a closed-shell-like configuration. Furthermore, structuring of the last shell towards the neighboring *N* atoms indicates *N*–*N* bonding.[26] The ring-like distribution of ELI around the Pb_4 tetrahedra indicates rather covalent interactions within the network. The picture is very similar to that in the Zintl-like compound K_4Pb_4 (Figure 4) with discrete Pb_4^{4-} anions.

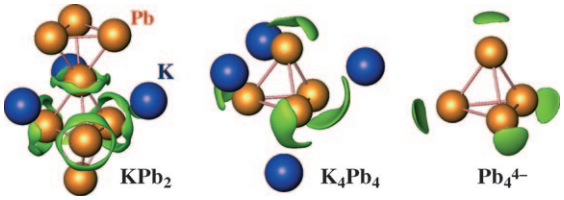

Figure 4. ELI isosurfaces around the Pb_4 tetrahedra in KPb_2 (see Figure 3), K_4Pb_4, and the isolated anion Pb_4^{4-}.

Despite the differences in the topology of ELI and different chemical composition of the phases discussed above, the total picture of the bonding also reveals similarities. The ELI maxima are localized mainly in vicinity of the *N* atoms; there are no maxima between the *M* atoms (Figure 2 and Figure 3). Stability of the structural patterns of Laves phases suggests a common driving force for realization of the closest packing motif with different chemical elements. To evaluate the role of the charge transfer as a possible driving force, the atomic charges were investigated by applying the quantum theory of atoms in molecules (QTAIM) approach.[27] Within this approach, the boundaries of an atom in a molecule or in a solid are defined through the zero-flux surfaces of the gradient field of the total electron density. Typical shapes of the QTAIM atoms in the Laves phases $CsBi_2$ and KPb_2 are shown in Figure 5. Integration of the electron density inside the region formed by the zero-flux surfaces (atomic basin) gives the charge of an atom (see Computational Methods).

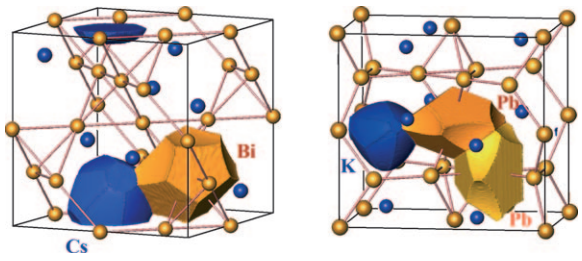

Figure 5. QTAIM atoms in the Laves phases $CsBi_2$ (structure type $MgCu_2$, left) and KPb_2 (structure type $MgZn_2$, right).

The maximal normalized charge transfer is limited to unity at the maximal electronegativity difference. For a variety of Laves phases MN_2, the normalized charge transfer from the *M* atoms to the *N* atoms is related to the difference between the electronegativities of the elements *N* and *M*. The electronegativity values from the scales of Sanderson[28] and Allred–Rochow[29] were utilized. The analysis of the relationship between the normalized charge transfer and the electronegativity difference (Figure 6) shows, despite a relatively

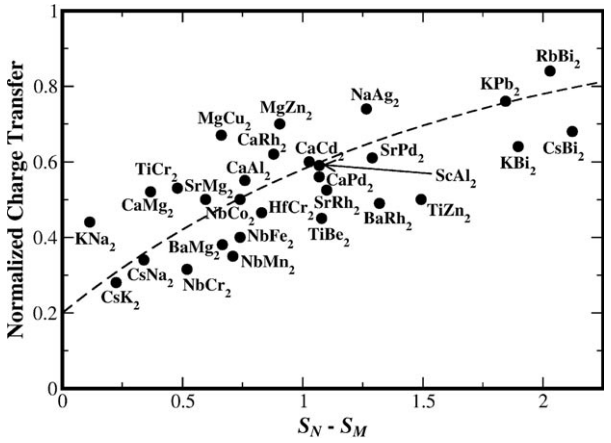

Figure 6. QTAIM charge transfer versus electronegativity difference for selected Laves phases shown for the Sanderson electronegativity scale. (Results for the Allred–Rochow scale (not shown) are similar.)

strong scattering of the data, the expected but not obvious general trend of charge-transfer increase with the electronegativity difference. $BaNa_2$[21] reveals small but reverse normalized charge transfer (−0.16) from *N* to *M*, which is in agreement with the Sanderson electronegativity scale but contradicts the Allred–Rochow scale, therefore requiring additional studies. The origin of the offset value of 0.2 is revealed by a calculation of the charge transfer for hypothetical compounds "KK_2", "$SrSr_2$", and "$NbNb_2$". Unexpectedly, the calculations for these homoatomic compounds reveal normalized charge transfers of approximately 0.2 from *M* to *N*. We consider this electronegativity-independent part as induced by structural topology.

This straightforward interpretation needs further elucidation however, as the significant charge transfer in, for example, the inter-alkali metal compounds (almost 0.5 for KNa_2) is surprising and puzzling. A closer inspection of the QTAIM atomic volumes of the alkali metals reveals enormous differences for the same kind of atoms in different phases. Just to mention the extremes: the potassium atom has a volume of 42 $Å^3$ and 86 $Å^3$ in KNa_2 and CsK_2, respectively, and the cesium atom is characterized by 67 $Å^3$ and 91 $Å^3$ in $CsNa_2$ and CsK_2, respectively. On the other hand, the QTAIM calculations for the binary compounds in the system Cs–K[30] showed that the volume of the cesium atom increases with its concentration, and that the Laves phase CsK_2 follows this trend in the system. Such large differences are only possible and meaningful in the case of a rather even electron density distribution between the atoms, as found in the elemental

metals themselves. This assumption was tested by comparing the valence electron densities in the basins of *M* and *N* atoms, which should differ only marginally. Indeed, if the respective core volumes (see Computational Methods) are subtracted from the QTAIM atomic volumes, the valence electron densities exhibit nearly identical values for the *M* and *N* atoms with a small difference in electronegativity. For the compounds KNa_2, $CsNa_2$, and CsK_2, valence electron density differences are calculated to be between *M* and *N* atoms of 0.00144 e Å^3, 0.00002 e Å^3, and 0.00241 e Å^3, respectively. For the Laves phases of *M* and *N* atoms greatly differing in the electronegativity, the valence electron density differences are an order of magnitude larger; for example, in $CsBi_2$ it is 0.08659 e Å^3. In combination with the ELI analysis, this indicates an increasing tendency towards formation of $N^{\delta-}$ anions. Thus, the crystal structure of KPb_2 is dominated by charge transfer to the polyanionic framework of corner- and face-condensed Pb_4 tetrahedra known as discrete anionic units from more cation-rich compound K_4Pb_4, or $K^+_4Pb_4^{4-}$ (Figure 4). The transformation from an intermetallic phase to a normal valence compound is even more pronounced in $KBi_{1.2}Pb_{0.8}$: The electron count for the $Bi_{2.4}Pb_{1.6}^{2-}$ tetrahedron is close to that in elemental phosphorus P_4, and the characteristic structural motif of the Laves phases, the condensed tetrahedra, distorts into discrete tetrahedral units.[31]

The ratio of valence electron densities in different atomic basins turns out to be another good measure for the characterization of chemical bonding in Laves phases (Figure 7). On the left hand side of the diagram, phases

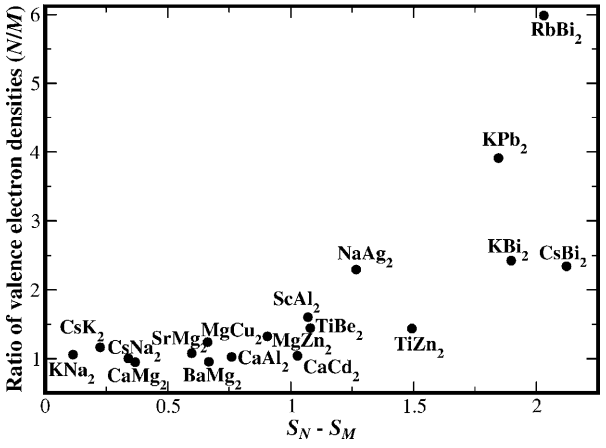

Figure 7. Valence electron density ratio versus electronegativity difference for Laves phases (Sanderson scale).

accumulate that exhibit a value of this ratio of almost unity. The charge transfer for the compounds is found to be rather small, and a multicenter bonding is revealed by ELI analysis. This type of interaction is very similar to the bonding found in the metallic elements that have an almost free-electron nature,[32] and is a necessary condition for the geometrical rule of size additivity that is obeyed by these phases. As in the charge density transfer, $BaNa_2$ also behaves oddly here (density ratio of 0.89 at $\Delta S = -0.08$ on the Sanderson scale). In this compound the stabilizing role must clearly be played by the (multicenter) heteronuclear covalent bonding. On the right hand side of the diagram, the value of the ratio of valence electron densities deviates significantly from unity, which is in agreement with the larger charge transfer detected for QTAIM atoms and indicates formation of $M^{\delta+}$ cations and $(N_2)^{\delta-}$ polyanions.

In conclusion, the study of the chemical bonding involved in the Laves phases by QTAIM and ELI/ED approaches shows that the diversity of the phases may be understood in terms of the electronegativity difference between *M* and *N* atoms. When this difference is small, the charge transfer from *M* to *N* is quite small. The corresponding Laves phases are characterized by multicenter bonding similar to that involved in elements. In contrast, when *N* is much more electronegative than *M*, the charge transfer from *M* to *N* is larger and the analysis of chemical bonding by ELI indicates the formation of polyanions $(N_2)^{\delta-}$.

Computational Methods

The chemical bonding analysis was based on first-principles electronic structure calculations. In this study, the full-potential non-orthogonal local orbital method (FPLO) with the recently implemented ELI module[33] is used. Topological analysis of ELI-D gives, along with the core electron regions, the ELI-D bond attractors and the corresponding bond basins through the zero-flux surfaces of the ELI-D gradient field.

Transfer of charge from the less electronegative to the more electronegative element in a binary compound is a generally accepted view. However, quantifying the relation between the amount of charge transfer and the electronegativity difference has proved to be elusive. Herein, we address this issue by proposing two approaches that are applicable only to binary Laves phases. The first is based on the atomic charges calculated according to QTAIM. In a Laves phase MN_2, the maximum amount of charge that can be transferred from the less electronegative *M* atom to the *N* network is the valence electron number of *M*, $Z^{val}{}_M$ (which is 1 for alkali metals and 2 for alkaline earth and transition metals). Since there are two *N* atoms in the formula unit, the maximum excess charge an *N* atom can get is $\Delta Q_{max} = Z^{val}{}_M/2$. The actual calculated charge transfer per *N* atom is defined as $\Delta Q_N = Q^{AIM}{}_N - Z_N$, where Z_N is the atomic number of *N* and $Q^{AIM}{}_N$ is the total charge contained in the atomic basin of *N*. We introduce the concept of normalized charge transfer, $f = \Delta Q_N/\Delta Q_{max}$. The relationship between *f* and the difference ΔS between the electronegativities S_N and S_M was investigated using two different electronegativity scales subject to the following conditions: 1) Due to the presence of geometry-driven charge transfer, *f* will be non-zero even when $\Delta S = 0$; 2) for large values of ΔS, *f* should tend to unity. This analysis suggests a relationship expressed by $f = 1-(1-f_{geom})e^{-\Delta S/\lambda}$, where f_{geom} is a number between 0.1 and 0.2. The parameter λ has different values for different electronegativity scales.

The formulation of a VEC-like idea using quantum mechanically calculable quantities is based on two observations: 1) the charge transfer due to electronegativity difference involves valence electrons only, and core electron numbers do not change; 2) our extensive ELI analyses show that core volumes of an element in different Laves phase compounds remain unchanged within 10%. Thus, ΔS affects mainly the valence electron count and the volume of the atomic valence region, which are quantities that can easily be calculated by combining QTAIM and ELI analyses. The QTAIM analysis yields an atomic volume V_M and charge Q_M for atom *M* in the compound; topological analysis of ELI-D gives atomic core volumes $V^{core}{}_M$, and for core charges nominal values $Z^{core}{}_M$ from the Aufbau principle can be used. Thus, a valence electron density can be defined as $D_M =$

$(Q_M - Z^{core}{}_M)/(V_M - V^{core}{}_M)$. The ratio D_N/D_M is thus expected to be very close to unity provided the electronegativity difference $\Delta S = S_N - S_M$ is not too large.

Received: March 14, 2010
Revised: June 22, 2010
Published online: October 7, 2010

Keywords: chemical bonding · electron density · electron localizabilty indicator · Laves phases

[1] R. Nesper, *Angew. Chem.* **1991**, *103*, 805; *Angew. Chem. Int. Ed. Engl.* **1991**, *30*, 789.
[2] G. J. Miller, *Eur. J. Inorg. Chem.* **1998**, 523.
[3] D. Fredrickson, S. Lee, R. Hoffmann, *Angew. Chem.* **2007**, *119*, 2004; *Angew. Chem. Int. Ed.* **2007**, *46*, 1958.
[4] E. Zintl, A. Harder, *Z. Phys. Chem. Abt. B* **1932**, *16*, 206.
[5] F. Laves, *Naturwissenschaften Z* **1939**, *27*, 65.
[6] G. E. R. Schulze, *Z. Elektrochem.* **1939**, *45*, 849.
[7] B. Böhm, W. Klemm, *Z. Anorg. Allg. Chem.* **1939**, *243*, 69.
[8] F. Laves, H. J. Wallbaum, *Z. Anorg. Allg. Chem.* **1942**, *250*, 110.
[9] Y. Ohta, D. G. Pettifor, *J. Phys. Condens. Matter* **1990**, *2*, 8189.
[10] F. Stein, M. Palm, G. Sauthoff, *Intermetallics* **2004**, *12*, 713.
[11] a) R. Haydock, R. L. Johannes, *J. Phys. F* **1975**, *5*, 2055; b) R. Nesper, G. J. Miller, *J. Alloys Compd.* **1993**, *197*, 109.
[12] R. L. Johnston, R. Hoffmann, *Z. Anorg. Allg. Chem.* **1992**, *616*, 105.
[13] a) C. Zhang, *Phys. B* **2008**, *403*, 2088; b) W. Chen, J. Sun, *Phys. B* **2006**, *382*, 279.
[14] Y. Kubota, M. Takata, M. Sakata, T. Ohba, K. Kifune, T. Tadaki, *J. Phys. Condens. Matter* **2000**, *12*, 1253.
[15] W. B. Pearson, *Acta Crystallogr. Sect. B* **1968**, *24*, 7.
[16] A. Simon, G. Ebbinghaus, *Z. Naturforsch. B* **1974**, *29*, 616.
[17] A. Simon, W. Brämer, B. Hillenkötter, H.-J. Kullmann, *Z. Anorg. Allg. Chem.* **1976**, *419*, 253.
[18] A. Simon, *Angew. Chem.* **1983**, *95*, 94; *Angew. Chem. Int. Ed. Engl.* **1983**, *22*, 95.
[19] C. D. Churcher, V. Heine, *Acta Crystallogr. Sect. A* **1984**, *40*, 291.
[20] O. Reckeweg, C. Lind, A. Simon, F. J. DiSalvo, *J. Alloys Compd.* **2004**, *384*, 98.
[21] G. J. Snyder, A. Simon, *Z. Naturforsch. B* **1994**, *49*, 189.
[22] U. Häußermann, S. Wengert, P. Hoffman, A. Savin, O. Jepsen, R. Nesper, *Angew. Chem.* **1994**, *106*, 2147; *Angew. Chem. Int. Ed. Engl.* **1994**, *33*, 2069.
[23] A. Savin, O. Jepsen, J. Flad, O. K. Andersen, H. Preuss, H. G. von Schnering, *Angew. Chem.* **1992**, *104*, 186; *Angew. Chem. Int. Ed. Engl.* **1992**, *31*, 187.
[24] a) M. Kohout, *Int. J. Quantum Chem.* **2004**, *97*, 651; b) M. Kohout, F. R. Wagner, Yu. Grin, *Int. J. Quantum Chem.* **2006**, *106*, 1499; c) M. Kohout, *Faraday Discuss.* **2007**, *135*, 43.
[25] A. Savin, B. Silvi, F. Colonna, *Can. J. Chem.* **1996**, *74*, 1088.
[26] a) M. Kohout, F. R. Wagner, Y. Grin, *Theor. Chem. Acc.* **2002**, *108*, 150; b) F. R. Wagner, V. Bezugly, M. Kohout, Yu. Grin, *Chem. Eur. J.* **2007**, *13*, 5724.
[27] R. F. W. Bader, *Atoms in Molecules: A Quantum Theory*, Oxford University Press, Oxford, **1999**.
[28] a) R. T. Sanderson, *J. Am. Chem. Soc.* **1983**, *105*, 2259; b) R. T. Sanderson, *Inorg. Chem.* **1986**, *25*, 1856; c) R. T. Sanderson, *Inorg. Chem.* **1986**, *25*, 3518; d) R. T. Sanderson, *Chemical Bonds and Bond Energy*, Academic Press, New York, **1971**.
[29] A. L. Allred, E. G. Rochow, *J. Inorg. Nucl. Chem.* **1958**, *5*, 261.
[30] Yu. Grin, A. Simon, A. Ormeci, *Mater. Res. Soc. Symp. Proc.* **2009**, *1128*, 1128-U08–01.
[31] S. Ponou, N. Müller, Th. F. Fässler, U. Häussermann, *Inorg. Chem.* **2005**, *44*, 7423.
[32] A. I. Baranov, M. Kohout, *J. Comput. Chem.* **2008**, *29*, 2161.
[33] A. Ormeci, H. Rosner, F. R. Wagner, M. Kohout, Yu. Grin, *J. Phys. Chem. A* **2006**, *110*, 1100.

